A&A 391, 911–915 (2002)
DOI: 10.1051/0004-6361:20020922
© ESO 2002

Astronomy & Astrophysics

Research Note

ISOPHOT far-infrared photometry of NGC 3079⋆

U. Klaas[1] and H. J. Walker[2]

[1] Max–Planck–Institut für Astronomie (MPIA), Königstuhl 17, 69117 Heidelberg, Germany
[2] CLRC, Rutherford Appleton Laboratory, Chilton, Didcot, Oxon OX11 0QX, UK

Received 13 June 2002 / Accepted 17 June 2002

Abstract. FIR photometry (from 15 μm to 200 μm) of NGC 3079 which is resolved by *ISOPHOT* at 60 μm is presented. With the assumption of an unresolved core plus an extended disk component, good consistency with *IRAS* and *SCUBA* data is found. The SED of the total flux between 60 μm and the submm can be modelled by the superposition of three dust components with temperatures of 32 K, 20 K and 12 K. The emission of the extended disk component is 1/3 of the unresolved core component in the 60–180 μm range, from 200 μm onwards its relative contribution increases. The resulting dust mass of 3.8×10^7 $M_\odot$ is consistent with a total gas-to-dust mass ratio of 200, close to the canonical value found for the Milky Way. These results demonstrate an appropriate way to disentangle and characterize the main dust components by combining *ISOPHOT* FIR data from the *ISO* Data Archive with submm data from *SCUBA*.

Key words. radiation mechanisms: thermal – astronomical data bases: *ISO* data archive – infrared: galaxies – galaxies: individual: NGC 3079 – galaxies: photometry

1. Introduction

NGC 3079 is an edge-on spiral galaxy with a LINER nucleus. It is highly inclined with an axis ratio of $7\farcm9 \times 1\farcm4$ and it shows large amounts of dust irregularly distributed throughout its disk with a large reddening towards its nucleus. A very detailed view of these features is presented on HST WFPC2 images published by Cecil et al. (2001). Being a source in the CfA Seyfert sample it became a target for FIR observations with *ISOPHOT* (Lemke et al. 1996) on the *Infrared Space Observatory (ISO)* (Kessler et al. 1996) to study the relative contribution by either an AGN or a starburst in heating the dust (Pérez García et al. 1998). Stevens & Gear (2000) combined IRAS and submm/mm observations with *SCUBA* and *IRAM* to construct its SED and reported that these data are inconsistent with the *ISO* data published by Pérez García et al. (1998). In particular the *ISO* 200 and 180 μm fluxes were in excess by a factor of 2–3 relative to those from their model fit. Since one of us (UK) is in charge of the overall *ISOPHOT* calibration consistency and the scientific validation of the *ISOPHOT* observing modes, we re-analyzed the *ISOPHOT* photometric data sets of NGC 3079 also taking into account the extended nature of the source with regard to the *ISOPHOT* resolution.

2. Observations and data reduction

ISOPHOT FIR observations of NGC 3079 were performed with the array cameras C100 (3×3 pixels, f.o.v. $138'' \times 138''$) at 60 μm and C200 (2×2 pixels, f.o.v. $184'' \times 184''$) at 120, 150, 180 and 200 μm, respectively. MIR observations at 15 and 25 μm were obtained with the aperture photometer using a $180''$ aperture. The *ISO* roll angle for these observations was 311 deg, so that the diagonals of the arrays ($3\farcm25$ for C100 and $4\farcm3$ for C200) were nearly parallel with the major axis of the galaxy. Due to the brightness of the source the observer did not perform a separate FIR background measurement.

We retrieved the data sets listed in Table 1 from the *ISO Data Archive* (Kessler et al. 2000) requesting on-the-fly reprocessing with the automatic data reduction pipeline OLP V10.0 using the calibration data set CALG V7.0. The *ISOPHOT* OLP data reduction steps are described in Laureijs et al. (2002). Typical calibration accuracies in staring mode for sources in the brightness range of NGC 3079 are better than ±15% (Klaas & Richards 2002). The chopped observations, which have been scientifically validated only with OLP V10.0 have a calibration accuracy of ±30% (Ábrahám et al. 2001; Klaas & Richards 2002).

Send offprint requests to: U. Klaas, e-mail: klaas@mpia.de

⋆ Based on observations with the Infrared Space Observatory ISO. ISO is an ESA project with instruments funded by ESA Member States (especially the PI countries France, Germany, The Netherlands and the UK) and with the participation of ISAS and NASA.

Article published by EDP Sciences and available at http://www.aanda.org or http://dx.doi.org/10.1051/0004-6361:20020922

Table 1. *ISOPHOT* data sets used for the NGC 3079 IR photometry.

product name	AOT	Comments
PPAP14300523.FITS	P03	chopped 180″ chop throw ⊥ main galaxy axis
PCAP14300524.FITS	P22	staring, no background measurement

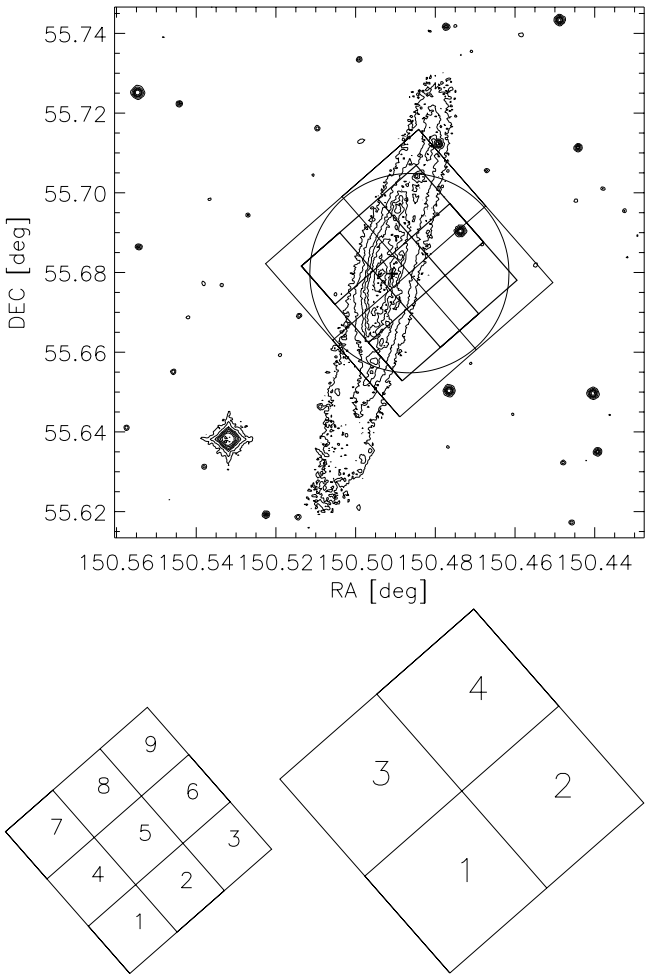

Fig. 1. Overlay of the *ISOPHOT* apertures on a contour plot of the *DSS2* red image. The C200 array (2 × 2 pixels) gives the outer bound, the PHT-P circular aperture is located inside it, circumscribing the C100 array (3 × 3 pixels). The cross westward of the optical intensity peak marks the position of the peak in the *SCUBA* maps from Stevens & Gear (2000). Below we indicate the relative positions of the C100 and C200 array pixels.

Figure 1 shows the positions and orientations of the *ISOPHOT* measurement apertures with regard to an optical image of the galaxy. It is obvious that the single pointings do not cover the complete galaxy, hence some flux loss, in particular for the C100 measurement, must be taken into account. The resulting flux on the arrays is very likely a mixture of a central unresolved source and extended disk emission. Furthermore, the central positions of the *ISOPHOT* apertures are shifted westward off the optical nucleus by 25″.

Table 2. FIR fluxes of NGC 3079 background derived from *COBE/DIRBE* weekly maps.

filter (μm)	*COBE* surface brightness (interpolated) (MJy sr^{-1})	integrated flux on *ISOPHOT* array (Jy)
60	8.0	5.55
120	3.5	6.90
150	2.8	5.08
180	2.6	4.67
200	2.4	3.88

Since no dedicated background measurement was performed, we estimated the background brightness in the FIR filters using the *COBE/DIRBE* weekly maps (Hauser et al. 1998). The surface brightness was integrated over the effective solid angle to derive the flux per pixel (Table 2). The background contribution makes up 4–5% of the total flux in the 120 to 200 μm range and 11.5% at 60 μm.

After background subtraction the fluxes were color corrected according to the fitted models of modified black bodies, see Table 3 for details. The color correction implies changes to the $\nu \times F_\nu$ = const. fluxes of less than 10%.

3. Results

The final *ISOPHOT* fluxes depend on the assumed source geometry. In the case of a point source a correction for the flux outside the array with the corresponding point spread function fraction has to be applied (this correction factor is implicitly applied by OLP, if the observer specified point source photometry). Below we derive fluxes for the condition that the FIR source was unresolved for *ISOPHOT* – this was assumed by Pérez García et al. (1998) – as well as by a simple approach to decompose an extended component from a central point source.

3.1. Point source photometry

Table 3 lists our photometry of NGC 3079, assuming that the flux comes exclusively from a point-source. While the 60 to 150 μm fluxes published by Pérez García et al. (1998) agree with ours within 25%, their 180 μm flux is too high by a factor of 1.4 and their 200 μm flux by a factor of 1.9. At the time when Pérez García et al. (1998) analysed these data sets, the standard products generated by the OLP (V6) were not yet scientifically valid. Therefore, they did an interactive processing using the *ISOPHOT* Interactive Analysis software (PIA) V6.1. It should be noted, however, that data products generated with OLP 6.3.2 on 15-Feb.-1998 yielded 180 and 200 μm fluxes within 15% of our new ones. This argues in favour of the general *ISOPHOT* calibration not being the source of error, but rather the individual interactive processing. Pérez García & Rodríguez Espinosa (2001) report fluxes for NGC 3079, reduced by them using PIA V7. Again the fluxes derived by them have been significantly influenced by their individual interactive processing;

Table 3. Combined integral IR and submm photometry of NGC 3079. References: SBNS89 = Soifer et al. (1989); BEA97 = Braine et al. (1997); SG00 = Stevens & Gear (2000); OLP10 = this work. IR fluxes are color corrected (cc) assuming SED shapes of modified black bodies. The OLP 10 fluxes are corrected for beam effects assuming a pure point source. The 850 μm and 1220 μm fluxes are corrected for contributions by the CO(3–2) and CO(2–1) lines.

λ_c (μm)	colour correction for SED shape	cc factor	cc fluxes (Jy)	reference
12	none	–	2.62	SBNS89
12	none	–	2.81	BEA97
15	λ^{-2} B (100 K)	1.026	1.80	OLP10
25	λ^{-2} B (100 K)	0.968	6.38	OLP10
25	λ^{-2} B (100 K)	0.933	3.84	SBNS89
25	λ^{-2} B (100 K)	0.933	3.79	BEA97
60	λ^{-2} B (30 K)	0.987	44.1	OLP10
60	λ^{-2} B (30 K)	0.899	55.8	SBNS89
60	λ^{-2} B (30 K)	0.899	58.7	BEA97
100	λ^{-2} B (30 K)	0.978	105.7	SBNS89
100	λ^{-2} B (30 K)	0.978	98.7	BEA97
120	λ^{-2} B (25 K)	1.000	135.7	OLP10
150	λ^{-2} B (22 K)	0.982	126.5	OLP10
180	λ^{-2} B (22 K)	1.034	97.1	OLP10
200	λ^{-2} B (22 K)	1.009	71.8	OLP10
450	none	–	7.86	SG00
850	none	–	1.14	SG00
1220	none	–	0.35	BEA97

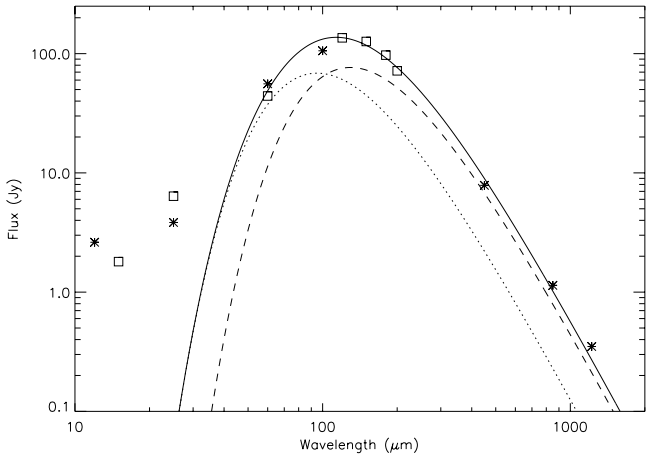

Fig. 2. Measured SED of NGC 3079 (total fluxes) from *IRAS*, *ISOPHOT*, *SCUBA* and *IRAM*. The meaning of the symbols is the following: asterisks: *IRAS* (12–100 μm), *SCUBA* (450 and 850 μm) and *IRAM* (1220 μm), squares: *ISOPHOT* point source photometry. *IRAS* and *ISOPHOT* fluxes are colour corrected, see Table 3 for details. The solid line is the superposition of two modified blackbodies ($\varepsilon \propto \lambda^{-2}$) with $T_1 = 30$ K (dotted curve) and $T_2 = 22$ K (dashed curve).

the 180 μm and 200 μm fluxes agree better with our fluxes, the 150 μm flux agrees less well.

In Fig. 2 we plotted the photometric data points and modelled the dust emission by the superposition of several modified ($\varepsilon \propto \lambda^{-2}$) black bodies. The dominant source beyond 100 μm is a 22 K component. In comparison with the *IRAS* photometry

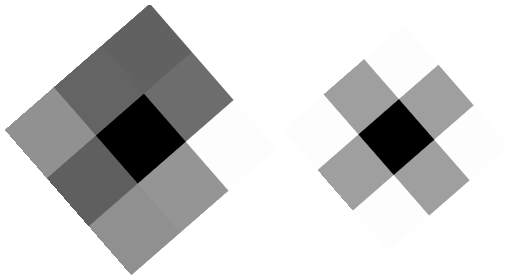

Fig. 3. Left: grey-scale representation of the logarithmic intensity distribution on the C100 array at 60 μm normalized to the peak flux (the lowest intensity level appears in white). The orientation of the array is like in Fig. 1, with pixel 1 at the bottom and pixel 9 at the top. Right: expected intensity distribution for a pure point source centered in pixel 5.

we notice that the *ISO* 60 μm flux is lower, as expected due to the less complete coverage of the source, however, the 120 and 150 μm fluxes are considerably (by 30%) above the total *IRAS* 100 μm flux. This is an indication that the correction factors applied for the point source PSF are too strong.

3.2. Decomposition of core and disk component

Figure 3 shows the intensity distribution on the C100 array which is clearly different from that of a pure point source. While there is a strong peak in the central pixel 5, in particular pixels 4, 8 and 9 show relatively strong excess emission, while pixel 3 shows no excess at all. All this can be understood from the location of the pixels relative to the plane of the galaxy (Fig. 1). For the decomposition of the core and disk component we followed a procedure described by Radovich et al. (1999):

$$F(i) = F_{\rm d}(i) + f_{\rm psf}(i) \times F_{\rm c}. \quad (1)$$

F(i) is the measured flux per pixel i, $F_{\rm d}(i)$ the disk component and $f_{\rm psf}(i) \times F_{\rm c}$ the fraction of the point source flux $F_{\rm c}$ scaled with the footprint of pixel i. The extended component in the central pixel 5 can be described as the average of the extended components in pixels 4 and 9 which are fully located on the disk:

$$F_{\rm d}(5) = (F_{\rm d}(4) + F_{\rm d}(9))/2. \quad (2)$$

This yields the following expression for $F_{\rm c}$:

$$F_{\rm c} = \frac{2 \times F(5) - F(4) - F(9)}{2 \times f_{\rm psf}(5) - f_{\rm psf}(4) - f_{\rm psf}(9)}. \quad (3)$$

We used the empirically determined $f_{\rm psf}(i)$ factors (Laureijs 1999) as listed in Table 4, however, they are strictly valid only for a source centered on pixel 5. This has some impact on the resulting photometric accuracy.

For the C200 array data this method does not work, because the point source is located at the edge of one pixel, close to the centre of the array. However, from the 60 μm results and the positional coincidence of C100 pixel 3 with the centre of C200 pixel 2 (Fig. 1), we can assume with reasonably good accuracy, that the C200 pixel 2 sees in essence the respective fraction

Table 4. 60 μm *ISOPHOT* photometry of NGC 3079 for core-disk decomposition: disk component per pixel $F_d(i)$ and total disk flux F_d, total core flux F_c and total flux F_{tot}. For comparison the *IRAS FSC* point source flux (F_c) and the total flux (F_{tot}) from Soifer et al. (1989) are given. Fluxes are not color corrected.

pixel	$F_d(i)$ (Jy)	f_{psf} (i)	F_c (Jy)	F_{tot} (Jy)
1	0.86	0.0038		
2	0.19	0.025		
3	−0.09	0.0038		
4	1.97	0.025		
5	2.20	0.667		
6	1.29	0.025		
7	0.83	0.0038		
8	1.70	0.025		
9	2.42	0.0038		
total	11.4		27.4	38.8
IRAS	5.7		44.5	50.2

Table 5. C200 *ISOPHOT* photometry of NGC 3079 for core-disk decomposition: total core flux F_c derived from flux in pixel 2, disk component F_d and total source flux F_{tot}. For comparison the 100 μm *IRAS FSC* point source flux (F_c) and the total flux (F_{tot}) from Soifer et al. (1989) are given. Fluxes are not color corrected.

λ_c (μm)	f_{psf} (array)	F_c (Jy)	F_d (Jy)	F_{tot} (Jy)
100 (IRAS)		89.2	14.2	103.4
120	0.489	75.7	25.8	101.5
150	0.552	74.8	24.9	99.7
180	0.601	61.3	21.8	83.1
200	0.667	35.1	23.6	58.7

of the PSF of the core component and only a negligible contribution by extended flux. Hence, we can use the intensity in this pixel to derive the relative point and extended source flux contributions in the other three pixels:

$$F_c = F(2) * 4/f_{psf}(array). \quad (4)$$

Here, f_{psf}(array) is the PSF correction for the whole array (Laureijs 1999). The resulting fluxes are listed in Table 5.

We note, that the total 120 μm *ISOPHOT* flux is now quite consistent with the total *IRAS* 100 μm flux. With regard to the flux derivation assuming a pure point source, the fluxes are reduced by 20–30%.

Figure 4 shows the SED for the total flux. We can model its shape by three modified blackbodies ($\varepsilon \propto \lambda^{-2}$). The strongest contributions come from a 32 K and a 20 K component. A weak 12 K component helps to flatten the slope longward of 500 μm and to better fit the submm/mm data. The 20 K component was not found by Stevens & Gear (2000), because they were lacking the information on the maximum of the SED. More recent work by Dunne & Eales (2001), combining SCUBA data with IRAS data for a range of galaxies, finds they need a two component dust model to fit to their data, with the cooler component having a temperature of 20–21 K.

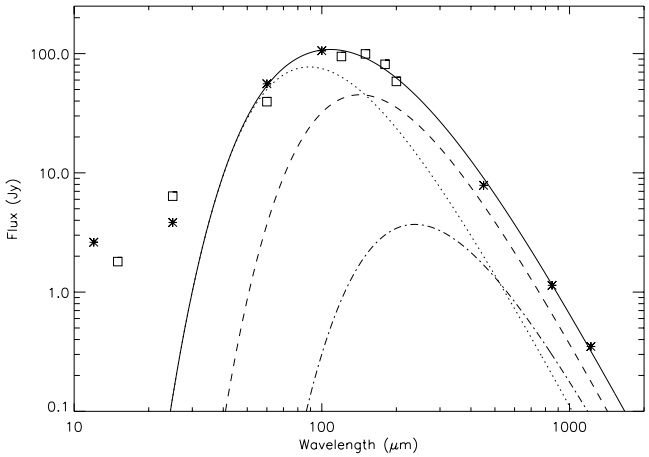

Fig. 4. Measured SED of NGC 3079 (total fluxes) from *IRAS*, *ISOPHOT*, *SCUBA* and *IRAM*. The meaning of the symbols is the following: asterisks: *IRAS* (12–100 μm), *SCUBA* (450 and 850 μm) and *IRAM* (1220 μm), squares: *ISOPHOT* photometry: sum of fluxes from an unresolved core and an extended disk component. *IRAS* and *ISOPHOT* fluxes are colour corrected (cc-factors: 60 μm: 0.980, 120 μm: 1.073, 150 μm: 1.004, 180 μm: 1.021, 200 μm: 1.004. The solid line is the superposition of three modified blackbodies ($\varepsilon \propto \lambda^{-2}$) with T_1 = 32 K (dotted curve), T_2 = 20 K (dotted curve) and T_3 = 12 K (dash-dotted curve).

4. Discussion

Although we do not have a complete map of NGC 3079, but only a single pointing (the goal of the observations was to measure the nuclear and circum-nuclear components), the *ISOPHOT* array camera pixels cover most of the area mapped by Stevens & Gear (2000) in the submm and Braine et al. (1997) in CO. Furthermore, the intensity distributions on the *ISOPHOT* arrays allows us to draw conclusions on the spatial distribution of the emission. The *FWHM* of a point source is about 20″ at 60 μm, corresponding to 1.5 kpc (D = 15 Mpc with H_0 = 75 km s^{-1} Mpc^{-1}). In the wavelength range 120–200 μm the *FWHM* is between 40″ and 67″ corresponding to 3–5 kpc. We therefore do not resolve the nuclear and circumnuclear regions. All extended emission we can resolve comes from larger radii. The flux ratio between the unresolved core and the disk component is roughly 3:1 from 60 to 180 μm. Only at 200 μm, close to the peak of the 12 K component, do we start to see a stronger contribution from the disk with the ratio being reduced to 1.5:1. The fluxes of the disk component are rather similar between 120 and 180 μm, suggesting that the 20 K component is relatively stronger here (cf. Fig. 4), however, for its 60 μm flux a contribution by the 32 K component is still necessary. At 200 μm the 12 K component becomes noticable. The temperature range found for the FIR SED is typical for dust heated by star formation (32 K) and for cirrus emission (20 K and 12 K). Since we do not resolve the nucleus, it is plausible that the SED reflects the existence of circumnuclear star formation, while the AGN component causes the excess

emission shortward of 60 μm. The images published by Cecil et al. (2001) show a major star forming complex about 7 kpc south of the nucleus. This significant star formation implies that a noticable 32 K dust component exists in the disk.

The 850 μm fluxes of the three dust components are 0.20 Jy (32 K), 0.65 Jy (20 K) and 0.30 Jy (12 K). Using

$$M_{\rm dust} = \frac{1}{\kappa_{850\ \mu{\rm m}}(\beta)} \cdot \frac{D^2 \cdot S_{850\ \mu{\rm m}}}{B_{850\ \mu{\rm m}}(T)} \quad (5)$$

with $\kappa^{\beta=2}_{850\ \mu{\rm m}} = 0.865\ {\rm cm}^2\ {\rm g}^{-1}$ (Klaas et al. 2001) this yields the following dust masses per component: $M_{\rm dust}(T = 32\,{\rm K}) = 2.7\times 10^6\ M_\odot$, $M_{\rm dust}(T = 20\,{\rm K}) = 1.7 \times 10^7\ M_\odot$, $M_{\rm dust}(T = 12\,{\rm K}) = 1.8 \times 10^7\ M_\odot$, hence $M^{\rm total}_{\rm dust} = 3.8 \times 10^7\ M_\odot$. This is only 1/3 of the dust mass derived by Stevens & Gear (2000), corrected for the different distance estimates. Adopting $M_{\rm HI} = 5.5 \times 10^9\ M_\odot$ from Braine et al. (1997) (their Table 1) and $M_{\rm mol.gas} = 2.2 \times 10^9\ M_\odot$ (their Sect. 4.3) yields a total gas mass of $M^{\rm total}_{\rm gas} = 7.7\times10^9\ M_\odot$ and hence a gas-to-dust mass ratio of 200, close to the canonical value for the Milky Way and the median value found for a large sample of normal galaxies (Stickel et al. 2000).

5. Conclusion

The FIR photometry of NGC 3079 between 100 and 200 μm published previously has to be revised. The *ISOPHOT* 60 μm photometry indicates the existence of an extended disk component and after decomposition of an unresolved core and the extended disk component, the fluxes are consistent both with *IRAS* at the short wavelength side and *SCUBA* at the long wavelength side. The SED of the total flux can be described by the superposition of three modified black bodies ($\varepsilon \propto \lambda^{-2}$) with temperatures of 32 K, 20 K and 12 K. The 32 and 20 K components are the dominant emission components. From the relative flux contribution of the three components a total dust mass of $3.8 \times 10^7\ M_\odot$ results, leading to a gas-to-dust ratio of 200. The dust masses related to the 20 K and 12 K components are quite similar. Between 60 and 180 μm the unresolved central component with a *FWHM* diameter between 1.5 and 4.5 kpc dominates the emission (3:1), while from 200 μm onwards the very cold dust in the disk leads to a stronger contribution of the disk. The results show the power of combined *ISOPHOT* and *SCUBA* observations in characterising the properties of cold dust. The results also demonstrate the quality of *ISOPHOT* OLP data products: for objects of this brightness range with calibration accuracies of better than ±15%, the products can be directly retrieved from the *ISO* Data Archive and used for scientific analysis.

Acknowledgements. The ISOPHOT Data Centre at MPIA is supported by Deutsches Zentrum für Luft- und Raumfahrt e.V. (DLR) with funds of Bundesministerium für Bildung und Forschung, grant No. 50 QI 0201. This research has made use of the Digitized Sky Survey, produced at the Space Telescope Science Institute, and the NASA/IPAC Extragalactic Database (NED), which is operated by the Jet Propulsion Laboratory, California Institute of Technology, under contract with NASA.

References

Ábrahám, P., Acosta-Pulido, J., Klaas, U., et al. 2001, Analysis of ISOPHOT chopped observations, Proc. Conf. The Calibration Legacy of the ISO Mission, ed. L. Metcalfe, & M. F. Kessler, ESA SP-481, in press

Braine, J., Guélin, M., Dumke, M., et al. 1997, A&A, 326, 963 (BEA97)

Cecil, G., Bland-Hawthorn, J., Veilleux, S., & Filippenko, A. V. 2001, ApJ, 555, 338

Dunne, L., & Eales, S. A. 2001, MNRAS, 327, 697

Hauser, M. G., Arendt, R. G., Kessel, T., et al. 1998, ApJ, 558, 25

Kessler, M. F., Steinz, J. A., Anderegg, M. E., et al. 1996, A&A, 315, L27

Kessler, M. F., Müller, T. G., Arviset, C., García-Lario, P., & Prusti, T. 2000, The ISO Handbook, vol. I: ISO – Mission Overview, version 1.0, November 24, 2000, SAI/2000-035/dc (ESA publications, Villafranca)

Klaas, U., & Richards, P. J. 2002, Report on the Scientific Validation of PHT OLP, version 10.0, version 1.0, 9-April-2002, `http://www.iso.vilspa.esa.es/users/expl_lib/PHT_list.html`

Klaas, U., Haas, M., Müller, S. A. H., et al. 2001, A&A, 379, 823

Laureijs, R. J. 1999, Point spread function fractions related to the ISOPHOT C100 and C200 arrays, version 1.0, 29-June-1999 (ISO Explanatory Library Doc.), `http://www.iso.vilspa.esa.es/users/expl_lib/PHT_list.html`

Laureijs, R. J., Klaas, U., Richards, P. J., Schulz, B., & Ábrahám, P. 2002, The ISO Handbook ESA SP-1262, vol. IV: PHT, The Imaging Photo-Polarimeter, version 2.0, July 8, 2002, SAI/1999-069/dc (ESA publications, Villafranca), `http://www.iso.vilspa.esa.es/manuals/HANDBOOK/pht_hb/`

Lemke, D., Klaas, U., Abolins, J., et al. 1996, A&A, 315, L64

Pérez García, A. M., Rodríguez Espinosa, J. M., & Santolaya Rey, A. E. 1998, ApJ, 500, 685

Pérez García, A. M., & Rodríguez Espinosa, J. M. 2001, ApJ, 557, 39

Radovich, M., Klaas, U., Acosta-Pulido, J., & Lemke, D. 1999, A&A, 348, 705

Soifer, B. T., Boehmer, L., Neugebauer, G., & Sanders, D. B. 1989, AJ, 98, 766 (SBNS89)

Stevens, J. A., & Gear, W. K. 2000, MNRAS, 312, L5 (SG00)

Stickel, M., Lemke, D., Klaas, U., et al. 2000, A&A, 359, 865